

# Linking the dynamics of chromatin occupancy and transcription with predictive models

Trung Q. Tran<sup>1</sup>, Vinay Tripuraneni<sup>2</sup>, Heather K. MacAlpine<sup>2</sup>, Sneha Mitra<sup>1</sup>,  
David M. MacAlpine<sup>2,3,\*</sup>, and Alexander J. Hartemink<sup>1,3,\*</sup>

<sup>1</sup>Department of Computer Science,

Duke University, Durham, NC 27708, USA

<sup>2</sup>Department of Pharmacology and Cancer Biology,

Duke University Medical Center, Durham, NC 27710, USA

<sup>3</sup>Center for Genomic and Computational Biology,

Duke University, Durham, NC 27708, USA

\*To whom correspondence should be addressed:

Tel: +1 919 681 6077, Email: david.macalpine@duke.edu

Tel: +1 919 660 6514, Email: amink@cs.duke.edu

July 3, 2020

## 1 **Abstract**

2 Though the sequence of the genome within each eukaryotic cell is essentially fixed, it  
3 exists in a complex and changing chromatin state. This state is determined, in part,  
4 by the dynamic binding of proteins to the DNA. These proteins—including histones,  
5 transcription factors (TFs), and polymerases—interact with one another, the genome,  
6 and other molecules to allow the chromatin to adopt one of exceedingly many possi-  
7 ble configurations. Understanding how changing chromatin configurations associate  
8 with transcription remains a fundamental research problem. We sought to character-  
9 ize at high spatiotemporal resolution the dynamic interplay between transcription and  
10 chromatin in response to cadmium stress. While gene regulatory responses to envi-  
11 ronmental stress in yeast have been studied, how the chromatin state is modified and  
12 how those modifications connect to gene regulation remain unexplored. By combining  
13 MNase-seq and RNA-seq data, we found chromatin signatures of transcriptional acti-  
14 vation and repression involving both nucleosomal and TF-sized DNA binding factors.  
15 Using these signatures, we identified associations between chromatin dynamics and  
16 transcriptional regulation, not only for known cadmium response genes, but across the  
17 entire genome, including antisense transcripts. Those associations allowed us to de-  
18 velop generalizable models that can predict dynamic transcriptional responses on the  
19 basis of dynamic chromatin signatures.

## 20 **Introduction**

21 Organisms require genic transcription to produce the proteins necessary for biologi-  
22 cal functions like growth, replication, repair, and response to environmental changes.  
23 Transcription is tightly regulated through the complex interplay of a myriad of DNA-  
24 binding factors (DBFs), including the histone octamers at the core of a nucleosome,  
25 transcription factors (TFs), and polymerases. These proteins and complexes involved  
26 in transcription, and the many others interacting with DNA, determine the chromatin  
27 landscape. How these constituents of the chromatin bind, unbind, move, and interact  
28 to regulate transcription remains an open area of research.

29 Many studies have made major strides in characterizing the roles of protein com-  
30 plexes involved in transcription. Chromatin immunoprecipitation (ChIP) has been used  
31 to assay binding sites of hundreds of proteins on a genomic scale, including factors in-  
32 volved in SAGA-dominated stress-related pathways and TFIID-dominated housekeep-  
33 ing pathways (Venters *et al.* 2011). Likewise, studies have probed proteins involved in  
34 the formation of the pre-initiation complex required for transcription initiation (Rhee  
35 and Pugh 2012). The role of numerous chromatin remodelers and their interactions  
36 have been characterized in detail through ChIP, proteomics, and gene expression anal-  
37 ysis of deletion mutants (Krogan *et al.* 2006; Lenstra *et al.* 2011; Shivaswamy and  
38 Iyer 2008; Weiner *et al.* 2012, 2015). However, these studies are constrained by lim-  
39 itations in their methods, including lack of antibodies for ChIP and viable deletion  
40 strains. Analysis is further complicated by the difficulty in disentangling direct chro-  
41 matin effects from the pleiotropic action of the many factors and remodelers occurring  
42 upstream of transcription. These aspects contribute to why the chromatin landscape  
43 involved in transcription is still poorly understood.

44 An alternative approach has been to profile chromatin occupancy in a protein-

45 agnostic manner using nuclease digestion. Digestion by a nuclease, such as micrococ-  
46 cal nuclease (MNase), provides a complementary perspective to understand chromatin  
47 occupancy as it can probe accessibility at base-pair precision. Recent genome-wide  
48 mapping studies have used nucleosome-sized MNase-seq fragments to characterize the  
49 dynamics of nucleosomes under various conditions, including the cell cycle (Nocetti  
50 and Whitehouse 2016), DNA damage (Tripuraneni *et al.* 2019), and heat shock (Teves  
51 and Henikoff 2011). Additionally, studies have attempted to understand the roles of  
52 the smaller DNA-bound factors that correspond to subnucleosomal MNase-seq frag-  
53 ments (Belsky *et al.* 2015; Brahma and Henikoff 2019; Chereji *et al.* 2017; Henikoff  
54 *et al.* 2011; Kubik *et al.* 2017; Ramachandran *et al.* 2017; Teves and Henikoff 2011).  
55 These studies highlight the challenge of characterizing the vast heterogeneity of—and  
56 interactions among—proteins and complexes involved in DNA-mediated processes, in-  
57 cluding transcription.

58 Factor-agnostic chromatin occupancy profiles from MNase provide an opportunity  
59 to link changes in chromatin occupancy at nucleotide resolution with transcriptional  
60 regulation, especially regulation induced by environmental perturbations such as cad-  
61 mium. Cadmium is a toxic metal whose deleterious effects have been well-characterized  
62 in yeast. Cadmium toxicity has been shown to induce proteotoxic stress (Faller *et al.*  
63 2005; Gardarin *et al.* 2010; Hartwig 2001; Sharma *et al.* 2008), oxidative stress (Bren-  
64 nan and Schiestl 1996), and inhibition of DNA repair systems (Jin *et al.* 2003). Yeast  
65 respond to cadmium exposure through the activation of stress response genes (Dormer  
66 *et al.* 2000; Hosiner *et al.* 2014; Jin *et al.* 2008) and the repression of ribosome biogene-  
67 sis and translation-related genes (Hosiner *et al.* 2014; Jin *et al.* 2008). While these cad-  
68 mium response pathways have been examined extensively through ChIP, proteomics,  
69 and transcription-related studies, the dynamics of a small subset of the chromatin re-  
70 sponse has only been inferred through deletion mutants or estimated through a limited  
71 set of ChIP antibodies.

72 Utilizing high-resolution spatiotemporal data, we developed general strategies to  
73 analyze, genome-wide, chromatin dynamics relative to changes in transcription. We  
74 exposed yeast to cadmium and collected data related to its chromatin and gene expres-  
75 sion state over a two-hour time course. This data allowed us to infer and differentiate  
76 essential cadmium stress response pathways solely from chromatin occupancy alone.  
77 We also identified chromatin changes associated with pervasive and potentially regula-  
78 tory antisense transcription. Our identification of unique classes of chromatin dynamics  
79 enabled us to develop a regression model that can predict the yeast's transcriptional re-  
80 sponse to cadmium.

## 81 **Results**

82 *Paired-end MNase-seq captures high-resolution chromatin occupancy dynamics associated*  
83 *with transcription during cadmium stress*

84 We sought to characterize the dynamics of chromatin in terms of changes in occupancy  
85 and organizational structure of nucleosomes as well as smaller transcription-related  
86 proteins. A nucleotide resolution view of chromatin occupancy dynamics in response  
87 to cadmium stress would allow us to associate and infer relationships between these  
88 chromatin changes with changes in transcription. Yeast cells were exposed to cad-  
89 mium and samples were collected over a two-hour time course (Fig. 1A). Chromatin  
90 occupancy and positioning dynamics were profiled using paired-end MNase-seq to map  
91 DBFs at base pair resolution (Fig. 1B). Concurrently, transcripts were interrogated us-  
92 ing strand-specific total RNA-seq (Fig. 1C).

93 To evaluate our data and methods, we analyzed the chromatin local to the well-  
94 characterized stress response gene HSP26 whose role is to facilitate the disaggregation  
95 of misfolded proteins (Cashikar *et al.* 2005). Hsp26 has been implicated in many stress  
96 conditions including heat shock (Benesch *et al.* 2010; Franzmann *et al.* 2008), acid-

97 ity (Kawahata *et al.* 2006), sulfur starvation (Pereira *et al.* 2008), and metals toxicity  
98 (Hosiner *et al.* 2014; Momose and Iwahashi 2001). Furthermore, several transcrip-  
99 tion factors, including Hsf1, Met4, and Met32, have been found to bind in HSP26's  
100 well-characterized promoter (Boy-Marcotte *et al.* 1999; Carrillo *et al.* 2012; Chen and  
101 Pederson 1993; Susek and Lindquist 1990; Treger *et al.* 1998). The context of these  
102 studies makes HSP26 a valuable gene to study in terms of its local chromatin dynamics  
103 in an activating condition.

104 We observe significant changes in the chromatin around HSP26's transcription start  
105 site (TSS) (Fig. 2A), coinciding with its increase in transcript level. Upstream, in  
106 HSP26's promoter, nucleosome-sized fragments of length 144–174 bp are replaced by  
107 small fragments less than 100 bp. In HSP26's gene body, nucleosome-sized fragments  
108 become “fuzzy”, increasing in positional and fragment-length variability (Fig. 2A). Nu-  
109 cleosomes in HSP26's promoter region are evicted (Lee *et al.* 2004) and replaced by  
110 an enrichment of factors associated with transcription initiation pushing nucleosomes  
111 downstream (Fig. 2B). Then, active transcription by RNA polymerases displaces and  
112 evicts nucleosomes (Kulaeva *et al.* 2010; Lee *et al.* 2004; Schwabish and Struhl 2004),  
113 which is apparent in our data in the significant loss of nucleosomal fragments within  
114 HSP26's gene body.

115 Because of these complex transcription-associated chromatin dynamics, we sought  
116 to quantify our MNase-seq data by summarizing the chromatin with two scores, which  
117 would also enable us to characterize subtle chromatin changes genome-wide, not just at  
118 genes with dramatic changes like HSP26. A “promoter occupancy” score was computed  
119 by counting the number of small fragments appearing in each gene's promoter region  
120 [–200, TSS] for each time point. We used a core promoter length of 200 bp as previ-  
121 ously described (Lubliner *et al.* 2013; Smale and Kadonaga 2003). As for the second  
122 score, because nucleosomes can be characterized by position changes and variance, in

123 addition to occupancy, a per nucleotide score was computed using a cross-correlation  
124 with a well-positioned, “idealized” nucleosome signal (Fig. 2C). We used the entropy  
125 of the +1, +2, and +3 nucleosome cross correlations to define the gene’s “nucleosome  
126 disorganization”. To handle variable RNA stability, we computed transcription rates  
127 using difference equations on the transcript levels and previously obtained decay rates  
128 (Geisberg *et al.* 2014; Miller *et al.* 2011; Presnyak *et al.* 2015).

129 Using these measures, we are able to succinctly track the coordination between  
130 HSP26’s chromatin dynamics and its increased transcription rate (Fig. 2D). Both of  
131 HSP26’s chromatin scores and its transcription rate increase dramatically throughout  
132 the time course and reach their peaks at 120 minutes. In addition to HSP26, we also  
133 examined the chromatin at genes with repressed (Supplemental Fig. 1) and unchanging  
134 (Supplemental Fig. 2) transcription contexts in response to cadmium and found similar  
135 linkages between changes in chromatin and transcription.

136 We next wanted to determine if this coordination exists genome-wide. The dynam-  
137 ics of the chromatin for each gene were further summarized into a single quantity.  
138 For each gene, their scores for promoter occupancy and nucleosome disorganization  
139 were transformed into a z-score and combined into an average across the time course  
140 (Fig. 3A, B). Sorting by this “combined chromatin” score, we observed a significant  
141 proportion of the genome exhibited a coordination between changes in chromatin and  
142 changes in transcription for genes that are both activated and repressed. A signifi-  
143 cant positive Pearson correlation of 0.49 was computed between the average change  
144 in promoter occupancy and the average change in transcription (Fig. 3C). Similarly, a  
145 correlation of 0.61 was found between the average change in nucleosome disorganiza-  
146 tion and the average change in transcription (Fig. 3D). When measuring the correlation  
147 between the average change in combined chromatin and change in transcription, an  
148 even higher correlation of 0.68 was computed (Supplemental Fig. 3A). This correlation

149 coupled with the lack of correlation (Supplemental Fig. 3B), at 0.17, between promoter  
150 occupancy and nucleosome disorganization themselves suggests that each metric pro-  
151 vides an orthogonal explanation of the chromatin relative to changes in transcription.

152 *Changes in nucleosome and small factor occupancy at TSSs recapitulate the cell's genome-*  
153 *wide transcriptional response to cadmium*

154 We next sought to determine how well chromatin dynamics reflect the cell's stress re-  
155 sponse to cadmium exposure. To answer this, we used the three, previously defined  
156 scores for chromatin dynamics: promoter occupancy, nucleosome disorganization, and  
157 combined chromatin. Using the 300 highest and lowest average scoring genes for each  
158 metric, using an approximately 90% inner percentile range, we performed Gene On-  
159 tology (GO) enrichment analysis to determine regulation pathways implicated under  
160 cadmium exposure. For each chromatin score, discrete GO enrichment pathways were  
161 identified with varying levels of false discovery rate (FDR) significance.

162 A well established response for cells undergoing stress involves shutting down ribo-  
163 somal and translation-related pathways (Hosiner *et al.* 2014; Reja *et al.* 2015; Vinay-  
164 achandran *et al.* 2018). We identified this repression through GO enrichment anal-  
165 ysis as genes with the greatest decreasing promoter occupancy, nucleosome disorga-  
166 nization, and combined chromatin scores. While, the combined score identifies the  
167 translation-related pathways with the greatest significance, many of the terms are re-  
168 covered with FDR less than  $10^{-10}$  by both promoter occupancy and nucleosome disor-  
169 ganization (Fig. 4A).

170 While ribosome and translation-related genes are repressed as a tightly regulated  
171 cluster, pathways activated under cadmium exposure are recovered with less signifi-  
172 cance, with FDRs less than  $10^{-4}$  (Fig. 4B). Consistent with cadmium and heavy metals  
173 stress studies, two major stress responses are activated under cadmium exposure: sul-

174 fur assimilation and protein folding (Faller *et al.* 2005; Fauchon *et al.* 2002; Hartwig  
175 2001). Each metric was able to identify distinct pathways with varying FDR. Promoter  
176 occupancy implicated sulfur assimilation and response to stress pathways with a FDR  
177 of  $10^{-3.9}$ , and nucleosome disorganization recovered protein refolding with an FDR of  
178  $10^{-2.1}$ . The combined chromatin score identified GO terms found distinctly in the pro-  
179 moter occupancy or nucleosome disorganization analyses, and for some terms with a  
180 better FDR, such as with sulfur amino acid metabolic process.

181 In both sets of GO analyses, using the combined chromatin score provides novel  
182 value in identifying implicated GO terms than using each individual metric alone. And  
183 though the cell's response to cadmium has been characterized through gene expression  
184 and ChIP-based studies, we show that elements of the chromatin alone are enough to  
185 accurately recover major cadmium response pathways.

### 186 *High-resolution time course recovers cascading induction of sulfur pathways*

187 As suggested by GO enrichment, significant chromatin changes occur at genes in the  
188 sulfur metabolic pathways. Utilizing chromatin and transcription data in our time  
189 course, we recover findings previously discovered through decades of ChIP, mutant,  
190 and transcription-related studies (Barbey *et al.* 2005; Blaiseau and Thomas 1998; Car-  
191 rillo *et al.* 2012; Cormier *et al.* 2010; Fauchon *et al.* 2002; Kuras *et al.* 1996, 2002;  
192 McIsaac *et al.* 2012; Ouni *et al.* 2010; Patton *et al.* 2000; Petti *et al.* 2012) and reveal  
193 novel details of the cascade of events regulating these pathways. Yeast cells exposed  
194 to cadmium require sulfur metabolized for biosynthesis of the cadmium-chelating glu-  
195 tathione (Fauchon *et al.* 2002). Genes in the sulfur metabolic pathways are activated  
196 primarily through the transcription factor Met4 and its binding complex, comprised of  
197 cis-binding factors Cbf1 and Met31/Met32, and accessory factor Met28 (Blaiseau and  
198 Thomas 1998; Kuras *et al.* 1996). Met4 is regulated through ubiquitination by SCF<sup>Met30</sup>

199 either targeting it for degradation or rendering into an inactive, but stable state (Bar-  
200 bey *et al.* 2005; Kaiser *et al.* 2000; Kuras *et al.* 2002). Cadmium exposure overrides  
201 this ubiquitination enabling Met4's functional activation of the sulfur metabolic genes  
202 (Barbey *et al.* 2005) (Fig. 5A). Using our calculated transcription rates and measures of  
203 chromatin dynamics, we recover three major components of the sulfur metabolic path-  
204 ways (Fig. 5B): (i) activation of the Met4 complex through its cofactors, (ii) activation  
205 of the sulfur pathways by Met4, and (iii) implicit down-regulation of Met4 activity by  
206 SCF<sup>Met30</sup>, evident in diminished transcription of Met4-regulated genes.

207       Upon deubiquitination, Met4 becomes functionally active and induces its own cofac-  
208 tors (Barbey *et al.* 2005; McIsaac *et al.* 2012). Concomitantly, MET32 is activated and,  
209 with Met4 through feedforward regulation, activates the sulfur metabolic genes (Car-  
210 rillo *et al.* 2012; McIsaac *et al.* 2012). In our time course, this induction is evident not  
211 only in increased transcription within 7.5 minutes for MET32 and MET28, but also in  
212 dramatic nucleosome disorganization in MET32's gene body, (Supplemental Fig. 4) and  
213 small fragment enrichment in MET28's promoter. Meanwhile, MET31's chromatin ex-  
214 hibits more unexpected behavior relative to its change in repressed transcription. While  
215 Met31 shares a binding motif and largely overlaps in function with Met32 (Blaiseau  
216 *et al.* 1997), Met31's role is not as prominent as Met32's in the activation of sulfur  
217 pathways (Carrillo *et al.* 2012; McIsaac *et al.* 2012; Petti *et al.* 2012). In our data, we  
218 observe that while MET31 is repressed, its nucleosomes disorganize with increased an-  
219 tisense transcription (Supplemental Fig. 5). Additionally, downstream of MET31's tran-  
220 scription end site (TES), small fragments become enriched at a Met31/Met32 binding  
221 motif. Taken together, our data identifies MET31 as a potential target for regulation  
222 through non-coding RNA (ncRNA) antisense transcription, a result we explore genome-  
223 wide in a subsequent section.

224       Following activation of MET32 and MET28, the Met4 complex is formed and acti-

225 vates genes in the sulfur pathways (Carrillo *et al.* 2012; McIsaac *et al.* 2012), which  
226 we also observe in the form of increased promoter occupancy, nucleosome disorgani-  
227 zation, and transcription. Each of the seven sulfur assimilation genes (Fig. 5C) and  
228 many of the downstream pathways increase in promoter occupancy and nucleosome  
229 disorganization within 15 minutes.

230 Additionally, Met4 induces a sulfur-sparing transcriptional-switch between func-  
231 tionally similar isoforms to indirectly contribute sulfur required for chelation. This  
232 switch includes replacing sulfur-rich Pdc1 with sulfur-lacking Pdc6, Ald4 with Ald6,  
233 and Eno1 with Eno2 (Fauchon *et al.* 2002). Each of these sulfur-lacking genes show  
234 evidence of activation in both their chromatin and transcription and, consistent with  
235 known studies (Fauchon *et al.* 2002), the most dramatic changes are evident as small  
236 fragment occupancy changes in PDC6 (Supplemental Fig. 6), PDC1 and ENO1's pro-  
237 moter.

238 Following the induction of the sulfur pathways, Met32 and Met4's activating func-  
239 tions diminish. Because prolonged activity of Met32 and Met4 induces cell cycle arrest,  
240 regulation of Met4 and Met32 through SCF<sup>Met30</sup> is required for long-term cell prolifer-  
241 ation (Ouni *et al.* 2010; Patton *et al.* 2000). These events are present most clearly in  
242 the chromatin dynamics for MET30 and MET32. We observe increasing transcription  
243 and gradual disorganization of gene body nucleosomes through the 120-minute time  
244 course. Additionally, we observe evidence for Met4 facilitating regulation of MET32  
245 (Ouni *et al.* 2010) through a plateau of MET32's nucleosome disorganization and tran-  
246 scription from 60–120 minutes.

247 Taken together, we are able to detail the timing of the activation of the Met4 com-  
248 plex, induction of the sulfur genes, and subsequent down-regulation of Met4 activity  
249 (Fig. 5D). This analysis complements established transcriptional studies by detailing  
250 chromatin dynamics of the sulfur metabolic pathways and identifying a potentially

251 novel regulatory mechanism for MET31 through antisense transcription.

252 *Cadmium treatment induces chromatin dynamics as distinct temporal clusters, including*  
253 *those linked to antisense transcription*

254 Our results demonstrate that the temporal order of chromatin changes were tightly as-  
255 sociated with the transcriptional regulation of sulfur pathways. Additionally, we found  
256 examples in which chromatin dynamics may not strictly correlate with sense transcrip-  
257 tion. With these observations in mind, we sought to understand the timing of the  
258 chromatin dynamics associated with cadmium stress using hierarchical clustering. We  
259 identified eight clusters, to identify generalized patterns, among 832 genes, chosen  
260 because they were among the 500 most dynamic in either promoter occupancy or nu-  
261 cleosome disorganization (some genes were in both, which is why there are fewer than  
262 1000; Fig. 6A). GO enrichment analysis was then performed on each cluster. Cluster-  
263 ing and GO enrichment analysis revealed three major results: (i) the sulfur and protein  
264 folding pathways can be differentiated through the timing of changes in the chromatin,  
265 (ii) increased transcription may not always accompany nucleosome disorganization,  
266 and (iii) antisense transcription can explain anti-correlated chromatin dynamics.

267 GO analysis of the eight clusters reveals differences in the timing of the the protein  
268 folding and sulfur metabolic pathways (Fig. 6B. Cluster 1, enriched with sulfur assim-  
269 ilation and methionine metabolic process genes, show an increased and steady state  
270 of promoter occupancy and nucleosome disorganization, consistent with the previous  
271 results. In cluster 2, genes relating to ATPase activity and protein refolding are acti-  
272 vated between 7.5–15 minutes, repressed between 30–60 minutes, and reactivated by  
273 120 minutes, evident in the change in promoter occupancy, nucleosome disorganiza-  
274 tion, and transcription rate for the latter 10% of genes in the cluster, genes that can be  
275 differentiated further with a higher  $k$ . Clusters 1 and 2 show that not only does the  
276 chromatin recover activating stress response pathways, but it also differentiates their

277 temporal changes consistent with changes in transcription rate.

278 While most genes presented thus far have shown to have a positive correlation  
279 between their changes in each chromatin measure and their change in transcription,  
280 clusters 6–8 reveal an unexpected anti-correlated relationship. While the transcription  
281 of many of these genes are activated, these genes show either a decrease in promoter  
282 occupancy and increase in nucleosome disorganization (in clusters 5 and 6), or an in-  
283 crease in promoter occupancy and decrease in nucleosome disorganization (in clusters  
284 7 and 8). This suggest more complex chromatin dynamics at play than the directly  
285 correlated measures we previously described. An example of this complexity is present  
286 in cluster 7, where the gene coding for an endoplasmic reticulum membrane protein  
287 Mcd4 exhibits chromatin with counter-intuitively organized nucleosomes despite in-  
288 creased transcription. (Supplemental Fig. 7).

289 For genes in cluster 6, some of the anti-correlated phenomena can be attributed  
290 to the antisense transcription (Fig. 6C) previously identified in MET31. Antisense  
291 transcription presents itself genome-wide with varying changes in sense transcription  
292 (Fig. 7A). We observed two major phenomena consistent with existing studies with  
293 respect to antisense transcription. First, as identified in other environmental condi-  
294 tions (Kim *et al.* 2010; Till *et al.* 2018; Wilhelm *et al.* 2008), antisense transcription  
295 is induced pervasively in yeast undergoing cadmium stress. The distribution of genes  
296 with increased antisense transcripts monotonically skews towards more transcription  
297 through the 120-minute time course (Fig. 7B). Of the genes whose sense transcrip-  
298 tion is unchanging, we found 529 exhibit a four-fold increase in antisense transcription  
299 (Fig. 7C). The second phenomena we observed pertains to genes whose sense transcrip-  
300 tion have changed. Previous studies have found that antisense transcription to be asso-  
301 ciated with both repression or activation of target genes (Kornienko *et al.* 2013; Swamy  
302 *et al.* 2014; Till *et al.* 2018; Vance and Ponting 2014). Under cadmium stress, we identi-

303 fied 92 genes whose antisense transcripts increased with decreased sense transcription,  
304 such as with MET31 and UTR2, whose overexpression has been linked with endoplas-  
305 mic reticulum stress (Miller *et al.* 2010) (Supplemental Fig. 8). We found 125 genes  
306 increased in both sense and antisense transcription, including the gene YBR241C (Sup-  
307 plemental Fig. 9) coding for a vacuole localization protein (Wiederhold *et al.* 2009).  
308 These phenomena indicate that changes in the chromatin may not strictly be associated  
309 with transcription, at least not solely on the sense strand.

310 While chromatin dynamics are able to accurately recover and differentiate the tim-  
311 ing of known stress response pathways, new questions are raised when these dynamics  
312 are not strictly correlated with sense transcription. Complexities introduced by the het-  
313 erogeneity of DBF binding dynamics and interactions and transcription on the antisense  
314 strand indicates that a more complex model of the chromatin landscape is required in  
315 elucidating the relationship between chromatin behavior and gene expression.

### 316 *Chromatin occupancy changes are predictive of changes in gene expression*

317 We next sought to develop a model to quantify the relationship between our measures  
318 of the chromatin and changes in transcription. We constructed a Gaussian process  
319 regression model to predict the transcription at each time point based solely on chro-  
320 matin dynamics and the preinduction transcription levels at 0 min. We constructed  
321 four models to evaluate various inclusions of measures of the chromatin, including a  
322 “full” model incorporating nucleosome positional shift calls (Supplemental Fig. 10) and  
323 measures of chromatin relative to called antisense transcripts (Supplemental Fig. 11).

324 We evaluated each model using 10-fold cross-validation and the coefficient of de-  
325 termination ( $R^2$ ), as the model’s proportion of predictable variance (Fig. 8A). For  
326 each model excepting the intercept model, prediction performance becomes worse  
327 through the time course as the transcript level deviates from the 0 minute transcript

328 feature. However, models including features of the chromatin consistently outperform  
329 the model using 0 min transcript level alone. Nucleosome disorganization is more in-  
330 formative than promoter occupancy and, consistent with previous results, combining  
331 both metrics provides more predictive power than each alone. The full model is not  
332 the best between 7.5–15 minutes because prediction is mainly driven by 0 minute tran-  
333 script level early on (Fig. 8B). It outperforms all other model between 30–120 minutes  
334 maintaining an  $R^2$  greater than 0.4 two hours after the cell's exposure to cadmium  
335 (Fig. 8C, D).

336 While our metrics do not describe the full state and variability of the chromatin  
337 landscape during transcription, our regression model provides evidence that a propor-  
338 tion of transcription can be explained from modifications of the chromatin state. This  
339 model serves as a baseline for understanding a portion of the complex relationship  
340 between the chromatin and transcription with numerous opportunities for extension.

## 341 Discussion

342 In contrast to CHIP-based studies, our study surveys the occupancy of DBFs across the  
343 entire genome without explicit information on the identities of the DBFs. While nu-  
344 cleosomes are well-characterized by nuclease digestion studies, profiling TFs and com-  
345 plexes that affect gene expression is a more challenging, open problem. Studies have  
346 identified the dynamics of various promoter-binding factors including transcription fac-  
347 tors, general transcription factors, polymerases, mediator, SAGA, TFIID, histone mod-  
348 ifications, chromatin remodelers, and others (Chereji *et al.* 2017; Huisinga and Pugh  
349 2004; Reja *et al.* 2015; Rhee and Pugh 2012; Shivaswamy and Iyer 2008; Venters *et al.*  
350 2011; Vinayachandran *et al.* 2018; Weiner *et al.* 2012, 2015). Utilizing both literature  
351 and motif analysis of TFs, we can implicitly describe the activity evident within gene  
352 promoters, such as with HSP26. Additionally, well-characterized responses, such as the

353 sulfur pathways, allow for additional context in determining the logical sequencing of  
354 chromatin modification events and modal changes in gene expression.

355 Analysis of the gene encoding Met4 cofactor Met31 uncovered chromatin changes,  
356 not only linked with gene expression, but also with antisense transcription. While per-  
357 vasive and regulatory ncRNA and antisense transcription have previously been shown  
358 to be associated with environmental perturbation (Camblong *et al.* 2007; Nadal-Ribelles  
359 *et al.* 2014; Swamy *et al.* 2014; Toesca *et al.* 2011), we characterized the relationship  
360 between these transcripts with gene expression from the perspective of the chromatin.  
361 Including the chromatin measures for the 667 genes with antisense transcripts also  
362 provides a marginal benefit in predicting sense transcripts (Fig. 8A). This benefit can  
363 be explored further by narrowing in on the effect size of these antisense-related chro-  
364 matin measures and by examining the individual sets of genes whose gene expression  
365 appears to have a relationship with antisense transcription.

366 Using the initial transcript level and chromatin dynamics of both sense and anti-  
367 sense transcription, our regression model is able to predict the level of sense transcript  
368 with an  $R^2$  greater than or equal to 0.44 for all time points following cadmium exposure  
369 Fig. 8A. There are multiple opportunities to extend this model. Further quantifying of  
370 the chromatin may include additional classes of fragments and characterization of the  
371 chromatin outside our defined  $[-200, 0]$  bp promoter and  $[0, 500]$  bp gene body. Addi-  
372 tionally, this data set enables opportunities for modeling using other statistical methods  
373 including generalized linear models, deep neural networks, or random forests. This  
374 model and its predictions serve as a baseline showing the potential modeling opportu-  
375 nities and richness of statistical power of the chromatin.

## 376 **Materials and Methods**

### 377 *Yeast strain*

378 The yeast strain used in this study has the W303 background with the genotype: MATa,  
379 leu2-3,112, trp1-1, can1-100, ura3-1, ade2-1, his3-11,15.

### 380 *Cell growth*

381 Cells were grown asynchronously in rich medium at 30°C to an OD<sub>600</sub> of 0.8. A sample  
382 was removed and crosslinked for MNase-seq and another was pelleted and flash frozen  
383 for RNA-seq at time 0 before the addition of CdCl<sub>2</sub> to a final concentration of 1mM.  
384 Samples were taken at 7.5 min, 15 min, 30 min, 60 min, and 120 min following CdCl<sub>2</sub>  
385 addition. All samples were taken and processed in duplicate.

### 386 *Chromatin preparation*

387 Chromatin was prepared as previously described (Belsky *et al.* 2015).

### 388 *RNA-seq*

389 RNA was prepared using the Illumina TruSeq Stranded Total RNA Human/Mouse/Rat  
390 kit (Cat number RS-122-2201) following the protocol provided by Illumina with Ribo-  
391 Zero.

### 392 *Sequencing library preparation*

393 Illumina sequencing libraries of MNase-treated DNA were prepared using 500 ng of  
394 DNA as previously described (Henikoff *et al.* 2011).

395 *Sequencing read alignment to the genome*

396 All reads were aligned to the sacCer3/R64 version of the *S. cerevisiae* genome using  
397 Bowtie 0.12.7 (Langmead *et al.* 2009). The recovered sequences from all paired-end  
398 MNase reads were truncated to 20bp and aligned in paired-end mode using the follow-  
399 ing Bowtie parameters: -n 2 -l 20 -m 1 -k 1 -X 1000.

MNase-seq duplicates,  $A$  and  $B$ , were randomly subsampled and merged to reduce bias from library preparation, sequencing, and MNase digestion.

$$A = \{a_0, a_{7.5}, a_{15}, a_{30}, a_{60}, a_{120}\}$$

$$B = \{b_0, b_{7.5}, b_{15}, b_{30}, b_{60}, b_{120}\}$$

Separately for each duplicate, the time point with the fewest reads determined the subsampling depth ( $k_A$  and  $k_B$ ):

$$T = \{0, 7.5, 15, 30, 60, 120\}$$

$$k_A = \min_{t \in T} |a_t|, \quad k_B = \min_{t \in T} |b_t|$$

Each duplicate was then subsampled (uniformly at random) to its respective subsampling depth to form new sets  $A'$  and  $B'$ :

$$A' = \{a'_0, \dots, a'_{120}\}$$

$$B' = \{b'_0, \dots, b'_{120}\}$$

$$|a'_t| = k_A, \quad |b'_t| = k_B, \quad \forall t \in T$$

Finally, the subsampled duplicates were merged into a superset,  $M$ , for downstream analysis:

$$M = \{m'_0, \dots, m'_{120}\} = \{a'_0 \cup b'_0, \dots, a'_{120} \cup b'_{120}\}$$

#### 400 *Selection of gene set*

401 We compiled a set of 4,427 genes for analysis. Genes were chosen according to five  
402 criteria: (i) classified as either verified or uncharacterized by sacCer3/R64, (ii) contains  
403 an open reading frame (ORF) at least 500 bp long, (iii) contains an annotated TSS, (iv)  
404 has an estimated half-life value, and (v) has adequate MNase-seq coverage.

405 Genes whose ORFs are less than 500 bp (Supplemental Fig. 12A) long were omitted  
406 in order to ensure valid “gene body” calculations between [TSS, +500]. TSS annota-  
407 tions were determined by (Park *et al.* 2014). For four important sulfur-related genes,  
408 Sul1, Sul2, Met32, and Hsp26, TSS annotations were manually annotated to be con-  
409 sistent with this study’s RNA-seq data. A half-life was required for each gene in order  
410 to estimate valid transcription rates. MNase-seq coverage was computed in a 2,000 bp  
411 window centered on each gene’s TSS. A position in this window is considered “covered”  
412 when there exists at least one read whose center lies on this position. MNase coverage  
413 was then defined as the number of covered positions in this window divided by the  
414 the length of the window, 2,000 bp. Genes with MNase coverage below 0.85 ( $n=109$ )  
415 were excluded from further analysis (Supplemental Fig. 12B).

#### 416 *Classification of MNase-seq fragments and occupancy*

417 For each gene, two regions were defined relative to their TSS. The promoter region was  
418 defined as a 200 bp region upstream of the TSS, [-200, TSS]. This region was chosen  
419 as a length previously described by (Lublinter *et al.* 2013; Smale and Kadonaga 2003).  
420 The gene body region was defined as the 500 bp region downstream of the TSS, [TSS,  
421 +500], to include the +1, +2, and +3 nucleosomes.

422 To compute metrics against nucleosome and small factor binding signals, two ref-  
423 erence data sets were used. Nucleosome-related metrics were computed by examining

424 the MNase-seq fragment distribution at 2,500 unique nucleosome positions mapped by  
425 a highly sensitive chemical mapping methodology (Brogaard *et al.* 2012). Small factors  
426 metrics were computed using 279 Abf1 binding sites determined through phylogenetic  
427 conservation and motif discovery obtained from [http://fraenkel-nsf.csbi.mit.edu/improved\\_map/p00](http://fraenkel-nsf.csbi.mit.edu/improved_map/p00)  
428 (MacIsaac *et al.* 2006). Prior studies have found clear signals of small MNase-seq frag-  
429 ment enrichment at Abf1 sites (Henikoff *et al.* 2011). MNase-seq distributions at each  
430 reference set was examined at 0 minutes, prior to cadmium treatment.

431 Reads were further delineated as nucleosome-sized fragments, those between 144–  
432 174 bp long, or small fragments, those less than 100 bp long. A mode length of 159 bp  
433 was computed at the MNase-seq fragments at (Brogaard *et al.* 2012) sites. A  $\pm 15$  bp  
434 range around this 159 bp mode length was chosen for nucleosome-sized fragments. A  
435 mode length of 75 bp was computed at (MacIsaac *et al.* 2006) sites. Fragments less  
436 than 100 were chosen to be small fragments. Occupancy was then defined by counting  
437 the number of fragment centers in these regions with the designated fragment lengths.  
438 Occupancy was calculated for small fragments in the promoter, nucleosome fragments  
439 in the promoter, small fragments in the gene body, and nucleosome fragments in the  
440 gene body.

#### 441 *Signal processing of chromatin*

442 A cross-correlation was computed in a similar manner described in (Tripuraneni *et al.*  
443 2019). Around each gene's TSS, a per bp cross-correlation score was computed to  
444 smooth the positional variation and filter out non-relevant fragments. Three two-  
445 dimensional cross-correlation kernels were constructed, an “idealized”, well-positioned  
446 nucleosome (Supplemental Fig. 13A) kernel, a clearly bound small factor kernel (Sup-  
447 plemental Fig. 13B), and a triple nucleosome “gene body” summarization kernel (Sup-  
448 plemental Fig. 13C). Each kernel was applied to the region local to each gene's TSS for

449 each time point to compute a per bp cross-correlation score (Supplemental Fig. 13D).

450 The nucleosome and small factor kernels were constructed using a bivariate Gaus-  
451 sian distribution parameterized by the mean and variance for the position and length  
452 for MNase-seq fragments. The parameters for each kernel were determined using the  
453 fragment length and position distributions at positions in (Brogaard *et al.* 2012) and  
454 (MacIsaac *et al.* 2006) previously described in *Classification of MNase-seq fragments and*  
455 *occupancy*.

456 To summarize the gene body chromatin as a whole, a three nucleosome, “triple”  
457 kernel was constructed to dampen the effect of the +1 nucleosome becoming more  
458 poised to be well-positioned (Nocetti and Whitehouse 2016). The triple nucleosome  
459 kernel was constructed by repeating the nucleosome kernel and increasing the vari-  
460 ance to take into account variable linker spacing. The nucleosome kernel spacing was  
461 determined using the average peak spacing between the [+1,+2] and the [+2,+3]  
462 nucleosome cross correlation scores Supplemental Fig. 13E.

#### 463 *Quantifying nucleosome disorganization*

For each gene, a random variable  $X$  was defined with  $n$  possible outcomes representing  
each position to evaluate relative to the gene TSS.

$$X = \{1, \dots, n\}$$

464 The probability of each outcome is estimated using the triple nucleosome cross corre-  
465 lation scores previously defined and normalized to sum to 1.

Because the triple kernel computes a score for three approximately adjacent nucleosome positions, we set  $n = 150$  to summarize the disorganization of the first three

nucleosomes in the gene body starting with +1 within the [0, 150] window.

$\text{cross}_{\text{nuc}}(i)$  = nucleosome cross correlation at  $i$

$$\hat{p}(X = x_i) = \frac{\text{cross}_{\text{nuc}}(i)}{\lambda}, \quad \text{where } \lambda = \sum_i^n \text{cross}_{\text{nuc}}(i)$$

Using this random variable, a score was computed for each gene to define its “nucleosome disorganization” using information entropy (Supplemental Fig. 13F):

$$H(X) = - \sum_{i \in 1 \dots n} P_X(x_i) \cdot \log_2 P_X(x_i)$$

#### 466 *Calling +1, +2, +3 nucleosomes*

467 Nucleosomes were called using the peak nucleosome cross correlation scores local to  
468 each gene’s TSS. The peak scores per bp of a 1000 bp window around the TSS were  
469 sorted, and with the largest peak iteratively removed. Positions within 150 bp around  
470 each peak were also removed and this value and position was called as a nucleosome.  
471 This procedure was repeated until all positions were removed and nucleosomes were  
472 called for this 1000 bp window.

473 “Linked” nucleosomes are defined as nucleosomes across the time course that nom-  
474 inally represent the same underlying nucleosome that may have changed in position  
475 or “fuzziness”. Nucleosomes were linked across time points using a nearest neighbor  
476 approach. In a greedy manner, the nucleosome the lowest disorganization score, the  
477 most well-positioned, was considered first. The position of this nucleosome was used to  
478 identify the linked nucleosomes in previous and subsequent time points by considering  
479 the nearest nucleosome for their respective time points within 100 bp of the original  
480 nucleosome’s position.

481 +1 nucleosomes were called by identifying linked nucleosomes closest to the TSS.  
482 +2 and +3 nucleosomes were computed as the next set of nucleosomes at least 80 bp  
483 downstream from their neighboring nucleosome.

484 *Gene Ontology enrichment analysis*

485 GO enrichment analysis was performed using GOATOOLS (Klopfenstein *et al.* 2018)  
486 with the go-basic.obo annotations from the Gene Ontology Consortium (Ashburner  
487 *et al.* 2000; The Gene Ontology Consortium 2019). False discovery rate was correcting  
488 using the Benjamini-Hochberg procedure (Benjamini and Hochberg 1995).

489 *Identification of transcription factor binding sites*

490 TF binding sites were identified with FIMO (Grant *et al.* 2011) using the motif database  
491 from MacIsaac *et al.* (2006) and default p-value threshold. Selected binding sites with  
492 supporting literature were annotated on typhoon plots.

493 *Transcription rate estimation*

As previously described in (Cashikar *et al.* 2005; Rabani *et al.* 2011; Yang *et al.* 2003),  
transcription rates were computed for each gene using a zero-order growth with first-  
order decay relationship:

$$\begin{aligned}\frac{dC_i}{dt} &= R_i - k \cdot C_i \\ C_i &= \frac{R_i}{k} + G_i \cdot e^{-kt_i} \\ t_i &\in \{7.5, 15, 30, 60, 120\}, \text{ s.t. } i \in \{1, \dots, 5\}\end{aligned}$$

Where  $C_i$  is the total RNA concentration measured by RNA-seq for sample  $i$ ,  $k$  is the  
fixed decay rate,  $G_i$  is the concentration of RNA affected by the zero order growth,  
and  $R_i$  is the unknown transcription rate. Assuming a constant rate of transcription  
between time points,  $R_i$  and  $G_i$  can be solved through pairs of difference equations:

$$\begin{aligned}C_{i-1} &= \frac{R_i}{k} + G_i \cdot e^{-k \cdot t_{i-1}} \\ C_i &= \frac{R_i}{k} + G_i \cdot e^{-k \cdot t_i}\end{aligned}$$

494 Transcription rates for  $R_i, i \in \{7.5, 15, 30, 60, 120\}$  were computed as systems of differ-  
495 ence equations between pairs of RNA-seq measurements to compute  $G_i$  and  $R_i$ .

Similarly, steady-state transcription rates,  $R_0$  at  $t_0$  were computed by setting the rate of production equal to the rate of decay:

$$t_0 = 0, i = 0$$

$$R_0 = k \cdot C_0$$

496 Decay rates were computed using the average half-life values,  $\tau$  between (Geisberg  
497 *et al.* 2014; Miller *et al.* 2011; Presnyak *et al.* 2015) and  $k = 1/\tau$ . Computed transcrip-  
498 tion rate values were then truncated to 0.1 TPM/min for valid fold-change evaluation.

#### 499 *Clustering of chromatin measures*

500 Clustering was performed using hierarchical clustering through SciPy (Virtanen *et al.*  
501 2020) for its flexibility in determining  $k$ . The Ward linkage was used for its efficient  
502 approximation to the minimal sum of squares objective (Ward 1963).

503 832 genes were chosen for clustering from the union of the 500 greatest increase  
504 in average promoter occupancy or 500 greatest increase in average nucleosome dis-  
505 organization, genes outside of an approximately 75% inner percentile range for each  
506 measure.

507 Clustering was performed against the pair-wise Euclidean distances between the  
508 z-score normalized measures of change in promoter occupancy and nucleosome dis-  
509 organization. Clustering to  $k=8$  was chosen to balance the interpretability of fewer  
510 clusters with the significance of identified GO terms in smaller, but more numerous  
511 clusters.

512 *Computing antisense transcription metrics*

513 Antisense transcript levels were quantified using a TPM calculation defined by (Wagner  
514 *et al.* 2012) for strand-specific RNA-seq reads on the antisense strand in the ORF for  
515 each gene.

516 TSSs and transcription end sites (TESs) for antisense transcripts were identified  
517 using RNA-seq pileup, the number of reads covering a genomic position. To increase the  
518 signal of fully transcribed transcripts, per-position pileup values were summed across  
519 each time point into a cumulative pileup and smoothed using a Gaussian kernel.

520 Antisense transcripts were identified starting with the highest cumulative pileup  
521 value within a gene's ORF on the antisense strand. The antisense TSS and TES were  
522 each identified by progressively searching upstream and downstream to identify the po-  
523 sitions in which the cumulative pileup values are minimized (Supplemental Fig. 11A).  
524 Antisense transcripts were not called if they did not meet a minimum threshold.

525 For the 667 genes in which an antisense transcript could be called (Supplemental  
526 Fig. 11B), nucleosome disorganization and promoter occupancy measures were com-  
527 puted, as previously described on the sense strand, relative to the antisense TSSs.

528 *Transcript level prediction model*

529 Gaussian process regression models were constructed to predict the  $\log_2$  transcript level  
530 for each time point using the  $\log_2$  transcript level at time 0, features of the chromatin  
531 at 0 minutes, and features of the chromatin for the time being predicted.

532 Four models were constructed to compare various combinations of measures of the  
533 chromatin: a small fragments promoter occupancy model, a gene body nucleosome  
534 disorganization model, a combined chromatin model, and a full model incorporating

535 all previous models' features with the addition of +1, +2, and +3 nucleosome position  
536 shift relative to 0 min (Supplemental Fig. 10) and measures of chromatin relative to  
537 called antisense transcripts (Supplemental Fig. 11).

538 Each Gaussian process regression model developed using `scikit-learn` (Pedregosa  
539 *et al.* 2011) with a radial-basis function (RBF) kernel with length scale bounded be-  
540 tween 0.1 and 100 and a white kernel with noise level  $10^{-4}$  as priors for covariance.  
541 The length scale bounds and noise parameters were determined empirically through a  
542 sensitivity analysis on a subset of the data.

543 Promoter occupancy and nucleosome disorganization measures were log transformed  
544 to an approximately normal distribution. Then, each chromatin measure, including  
545 nucleosome shift, was z-score normalized so that the RBF length parameter could be  
546 successfully approximated.

547 Performance for each model was evaluated using the coefficient of determination,  
548  $R^2$ , under 10-fold cross validation.

## 549 **Data Accession**

550 Code for this work is available at <https://github.com/HarteminkLab/cadmium-paper>.  
551 Data is available on NCBI/GEO with accession number GSE153609.

## 552 **Acknowledgments**

553 The authors would like to thank Yulong Li and Greg Crawford for their suggestions and  
554 helpful comments during the development of this research. The work was supported  
555 by the following grants from the NIH National Institute of General Medical Sciences:

<sup>556</sup> R35-GM127062 (D.M.M.) and R01-GM118551 (A.J.H.).

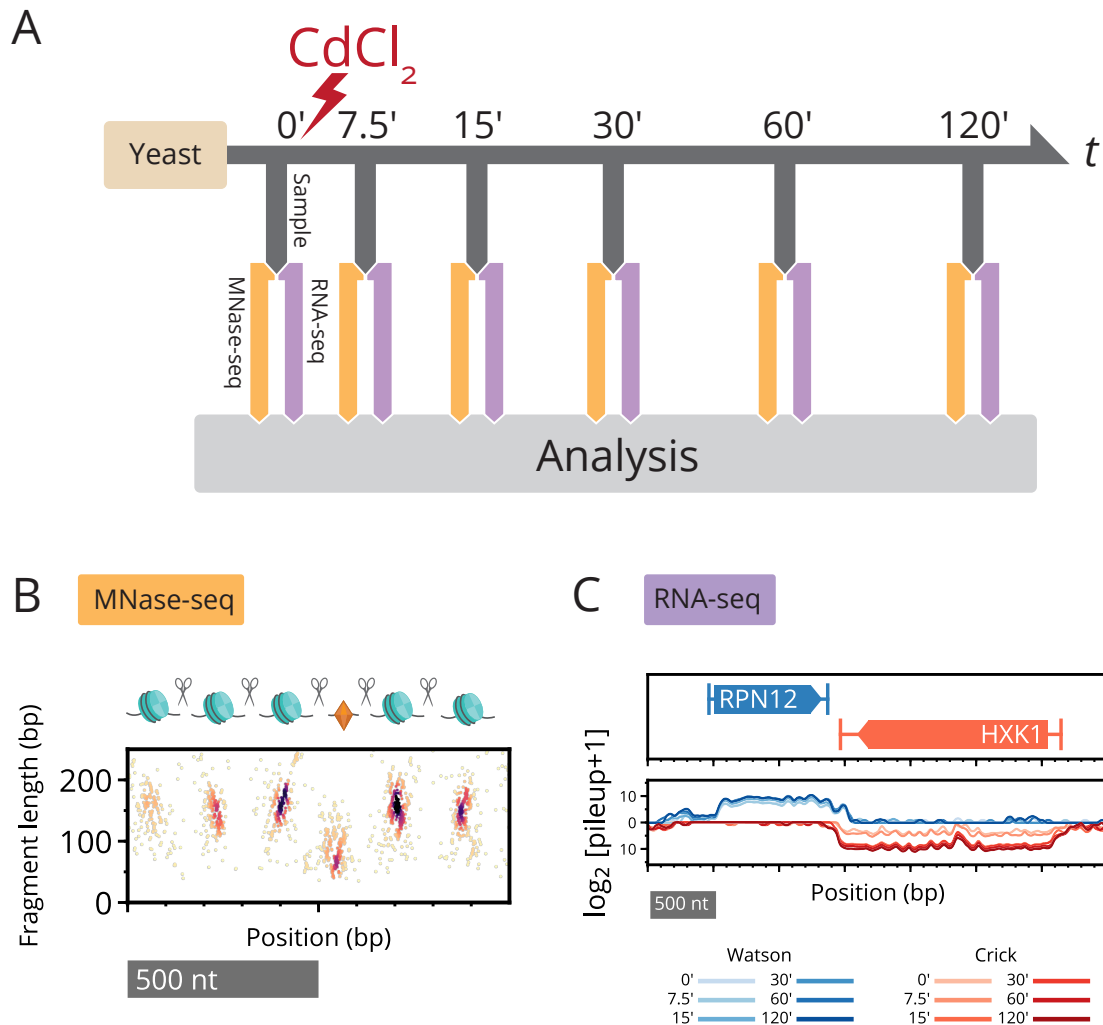


**Figure 1.** Paired-end MNase-seq and stranded RNA-seq capture high-resolution chromatin occupancy and transcriptome state throughout a perturbation time course. **(A)** Overview of cadmium perturbation experiment in which paired-end MNase-seq and strand-specific RNA-seq samples were collected immediately prior to cadmium exposure and for five additional time points over two hours. **(B)** Depiction of nucleosomes flanking a small (subnucleosomal) binding factor, and fragments that result upon digestion by MNase. Paired-end MNase-seq fragments are plotted based on their center position and length. **(C)** Strand-specific RNA-seq is plotted as the  $\log_2$  pileup, the number of total RNA-seq reads at each genomic position, separately mapped to Watson (blue) and Crick (red) strands. Changing RNA-seq read levels over the time course are plotted using progressive coloring for each strand.

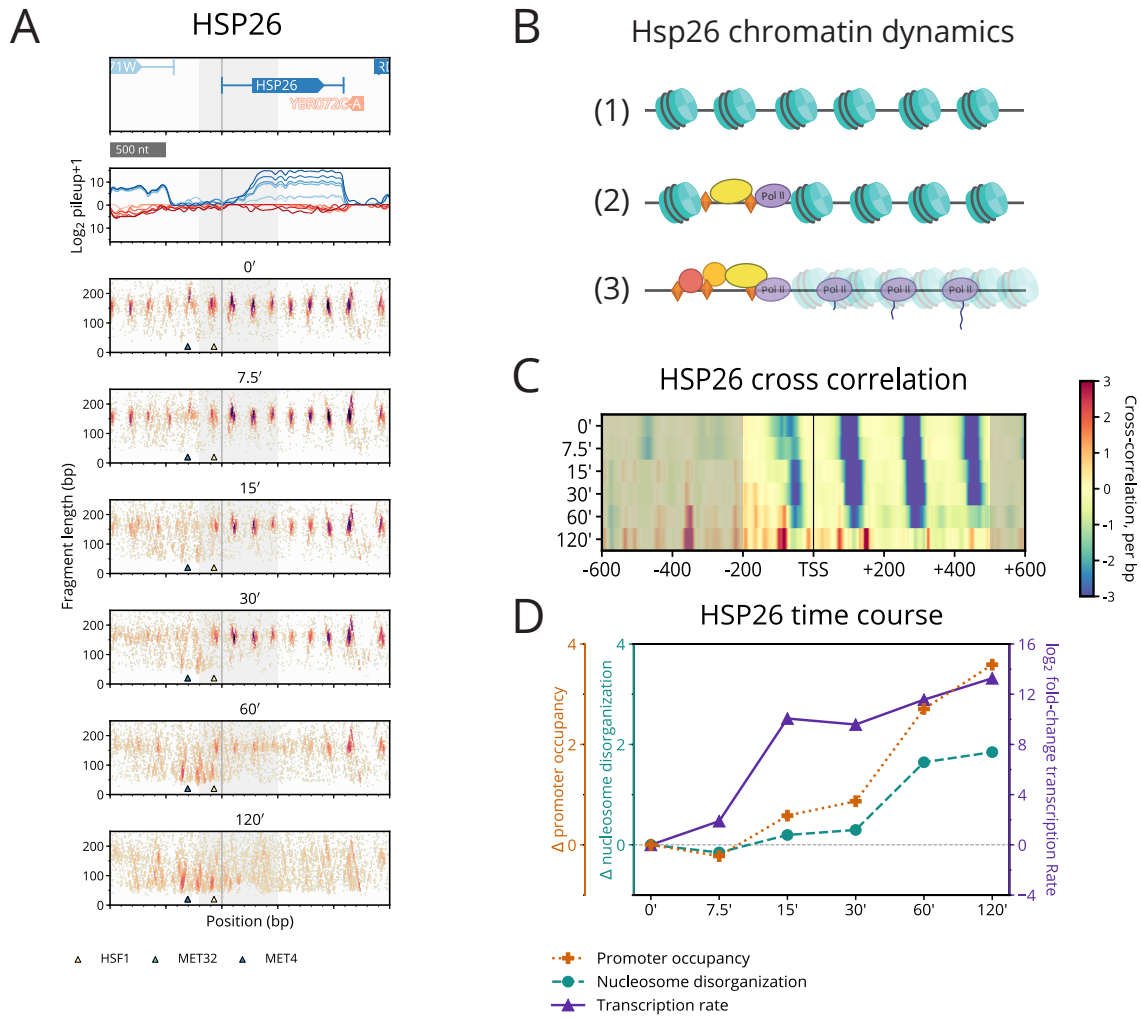


**Figure 2.** Cadmium induces local chromatin dynamics that correlate with transcription of HSP26. **(A)** Typhoon plot shows dynamics of MNase-seq and RNA-seq data near HSP26. Nucleosomes in the promoter region are replaced by small fragments, while gene body nucleosomes disorganize (grey shading highlights the  $[-200,500]$  region around the TSS that we analyze for all genes). Small fragments appear around motifs for known regulators Hsf1 (yellow triangle), Met4 (blue triangle), and Met32 (obscured by blue triangle) **(B)** Depiction of HSP26's chromatin dynamics. (1) Before treatment, nucleosomes are well-positioned. (2) Between 15–30 minutes, nucleosomes are evicted from the promoter region and replaced by transcription-related proteins and complexes. (3) By 60–120 minutes, nucleosomes are fuzzy and polymerases are actively transcribing HSP26. **(C)** Heatmap of differential cross-correlation values of HSP26 through time course, summarizing how gene body nucleosomes initially shift downstream and then disappear, and how promoter nucleosomes are rapidly displaced as small fragments accumulate. Higher values (more red) indicate higher cross-correlation with subnucleosome fragments; lower values (more blue) indicate a stronger signal for nucleosome fragments. **(D)** Line plot of HSP26 time course summarizing the change relative to 0 min in occupancy of promoter small fragments (orange), disorganization of gene body nucleosomes (turquoise), and transcription rate (purple).

557

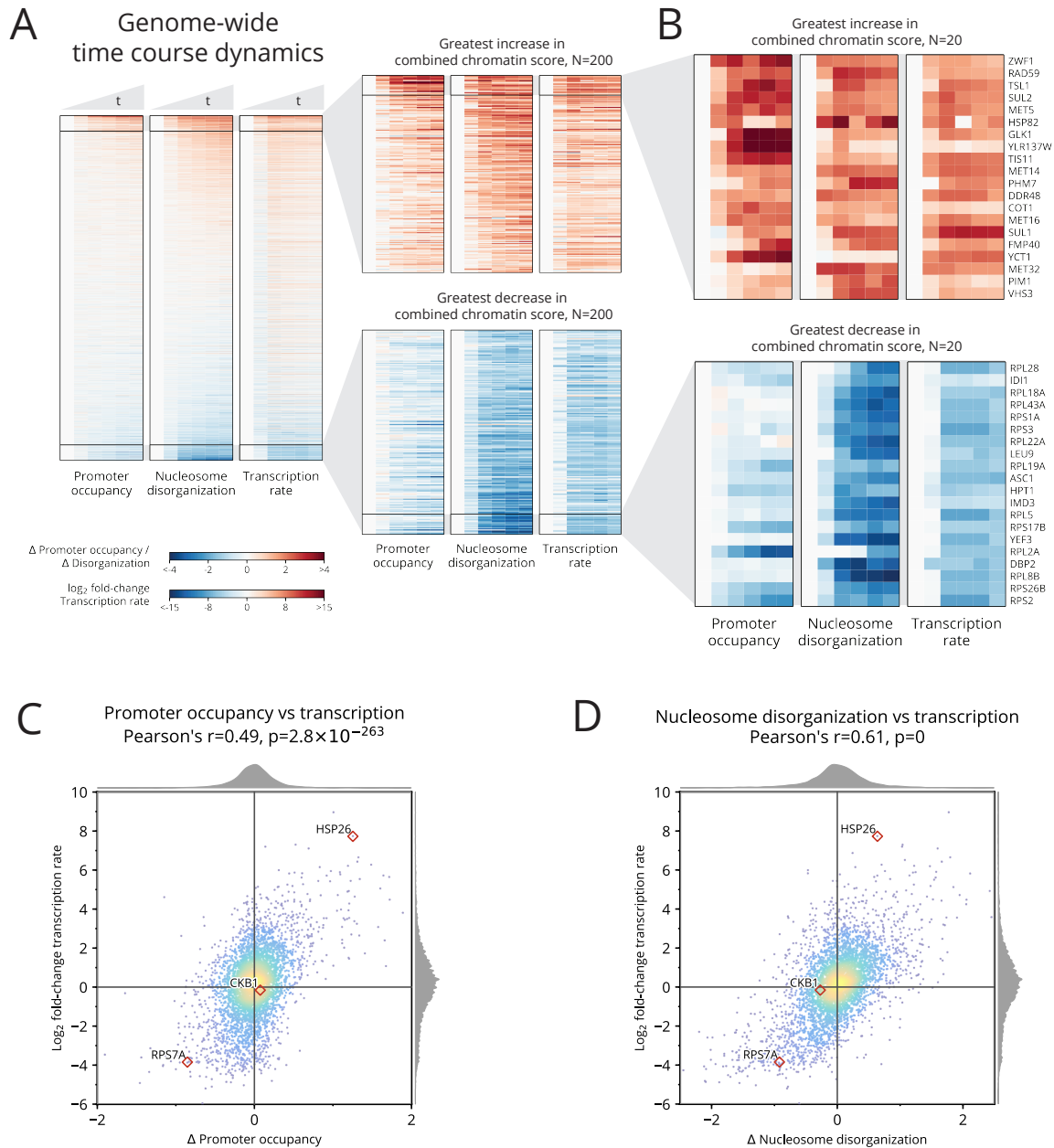


**Figure 3.** Cadmium induces genome-wide chromatin dynamics that correlate well with genome-wide transcriptional dynamics. **(A)** Heatmaps of changes in chromatin occupancy measures and transcription rate for all genes and all times, relative to 0 min (left: promoter small fragment occupancy; middle: gene body nucleosome disorganization; right: transcription rate). Genes (rows) are sorted by combined chromatin score. **(B)** Detailed heatmaps of the 20 genes whose combined chromatin scores increase (top) or decrease (bottom) most. **(C)** Scatter plot of relationship between change in promoter occupancy and change in transcription rate, each averaged over the time course. **(D)** Scatter plot of relationship between change in nucleosome disorganization and change in transcription rate, each averaged over the time course.

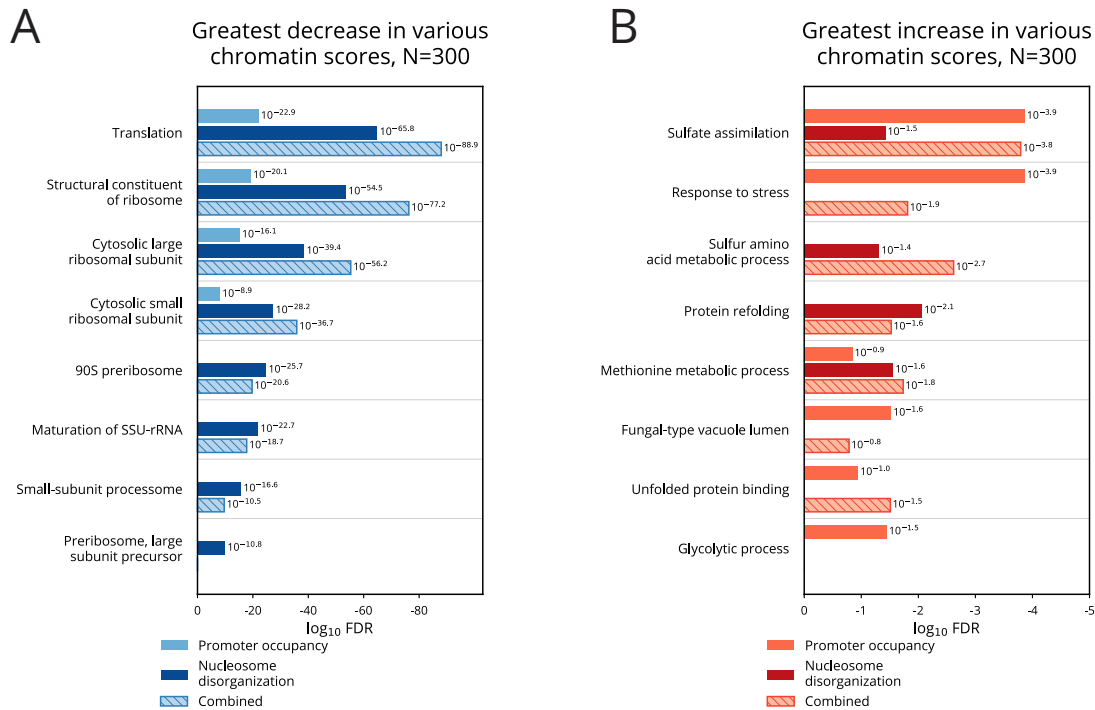


**Figure 4.** GO enrichment analysis of genes with highly dynamic chromatin support established cadmium response pathways. **(A)** GO enrichment analysis of 300 genes with greatest decrease in promoter occupancy, nucleosome disorganization, and combined chromatin score. Translation-related genes are recovered with significant FDR. **(B)** GO enrichment analysis of 300 genes with greatest increase in promoter occupancy, nucleosome disorganization, and combined chromatin score. Genes involved with stress response, sulfur assimilation, and protein folding pathways are recovered with significant FDR.

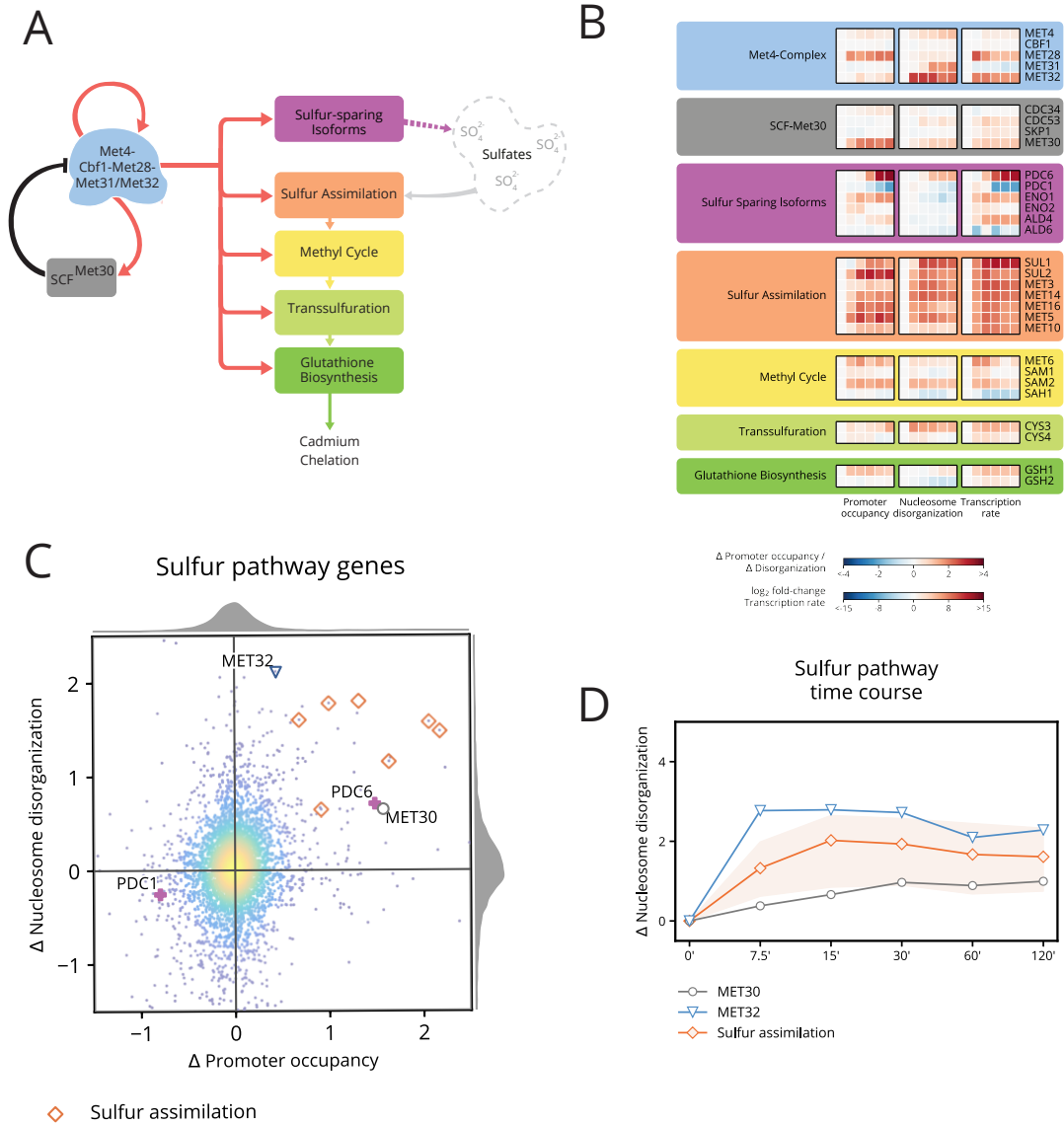


**Figure 5.** Chromatin and transcription dynamics detail Met4 and Met32 functional activation, induction of sulfur genes, and subsequent regulation. **(A)** Met4 complex activates cascading sulfur pathways required for cadmium chelation and is regulated by SCF<sup>Met30</sup> **(B)** Heatmap of changes in chromatin occupancy and transcription rate for the sulfur pathway genes. Cofactors of the Met4 complex exhibit dramatic chromatin changes in promoter occupancy (for MET28) and nucleosome disorganization (for MET32). Sulfur sparing isoforms exhibit inverse chromatin dynamics most pronounced between PDC6 and PDC1. Nearly all of the sulfur assimilation pathway have a dramatic increase in promoter small fragments and nucleosome disorganization. **(C)** Scatter plot of the average change in promoter occupancy and average change in nucleosome disorganization. Chromatin dynamics in sulfur-related genes may appear primarily through a change in a single measure of the chromatin, as with MET32 (blue triangle), MET30 (gray circle), and PDC6/PDC1 (violet), or as changes in both promoter occupancy and nucleosome disorganization, such as with the sulfur assimilation genes (orange diamonds) **(D)** Line plot of the change in nucleosome disorganization for the regulator gene MET30, activator MET32, and the sulfur assimilation genes—where the orange line represents the mean and the light orange region represents the entire range of values for the seven sulfur assimilation genes. Met4 complex cofactor MET32's disorganization is highest at 7.5 min while the sulfur assimilation genes and MET30, both of which are activated by the Met4 complex, reach their greatest nucleosome disorganization between 15–30 min.

558

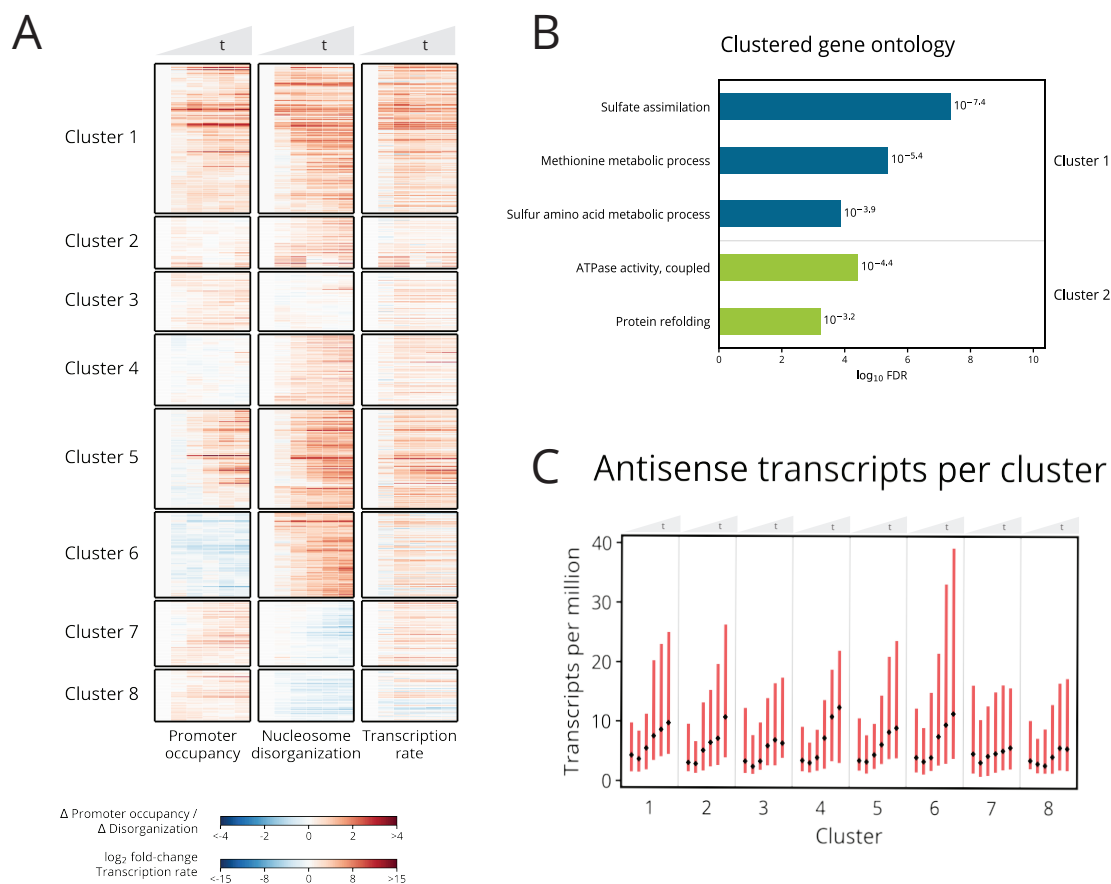


**Figure 6.** Small fragment promoter occupancy enrichment and gene body nucleosome disorganization reveal stress response pathway timing and patterns with antisense transcription. (A) Hierarchical clustering of 832 genes from the union of the 500 greatest increase in average promoter occupancy or 500 greatest increase in average nucleosome disorganization. Clusters 6–8 contain genes with anti-correlated chromatin dynamics. (B) GO enrichment analysis identifies clusters 1 and 2 for sulfur and protein refolding pathways respectively. (C) Antisense transcript level for each cluster across the time course. Cluster 6 shows enrichment of antisense transcripts matching increased nucleosome disorganization and decreased in promoter occupancy in A.

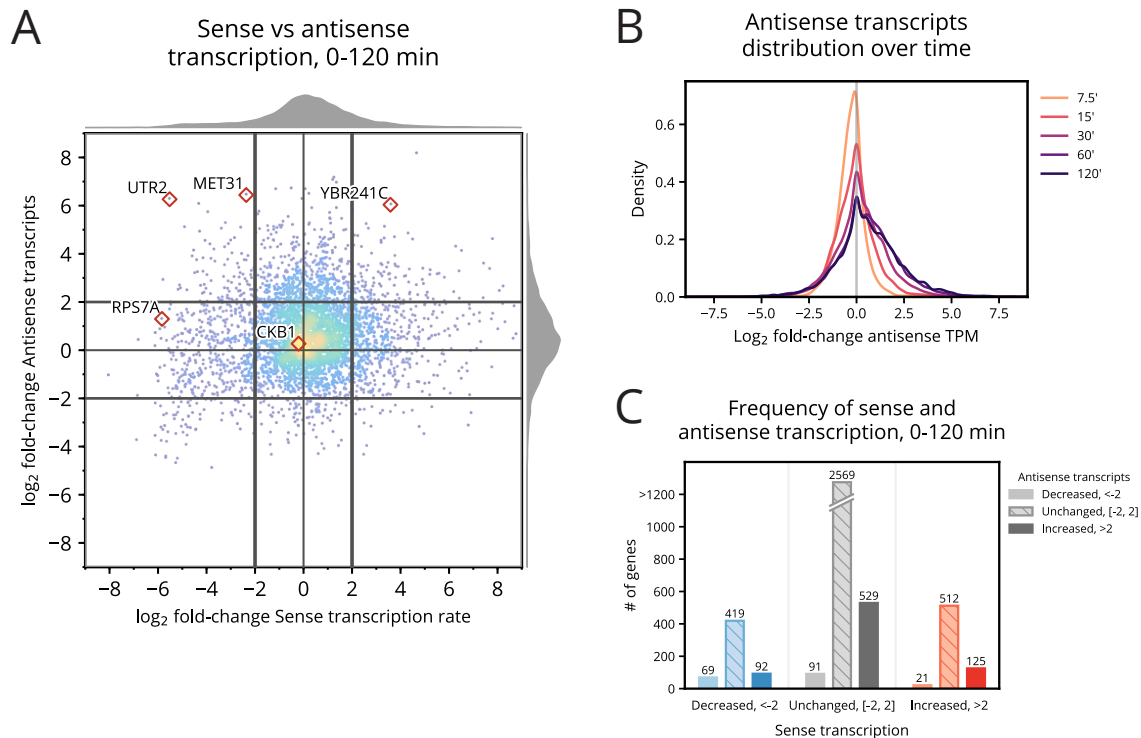


**Figure 7.** Cadmium induces changes in both sense and antisense transcription. **(A)** Distribution of the log<sub>2</sub> fold-change in sense transcription against the log<sub>2</sub> fold-change in antisense transcripts from 0–120 min. Antisense transcripts are enriched genome-wide by 120 min. **(B)** Distribution of the log<sub>2</sub> fold-change in antisense transcripts for each time point following 0 min. Antisense transcripts monotonically increase through the 120-min. **(C)** Counts of genes that exhibit decreased, unchanged, and increased sense and antisense transcripts from 0 and 120 minutes. Unchanging and increased sense transcription exhibit positively skewed enrichment of antisense transcripts.

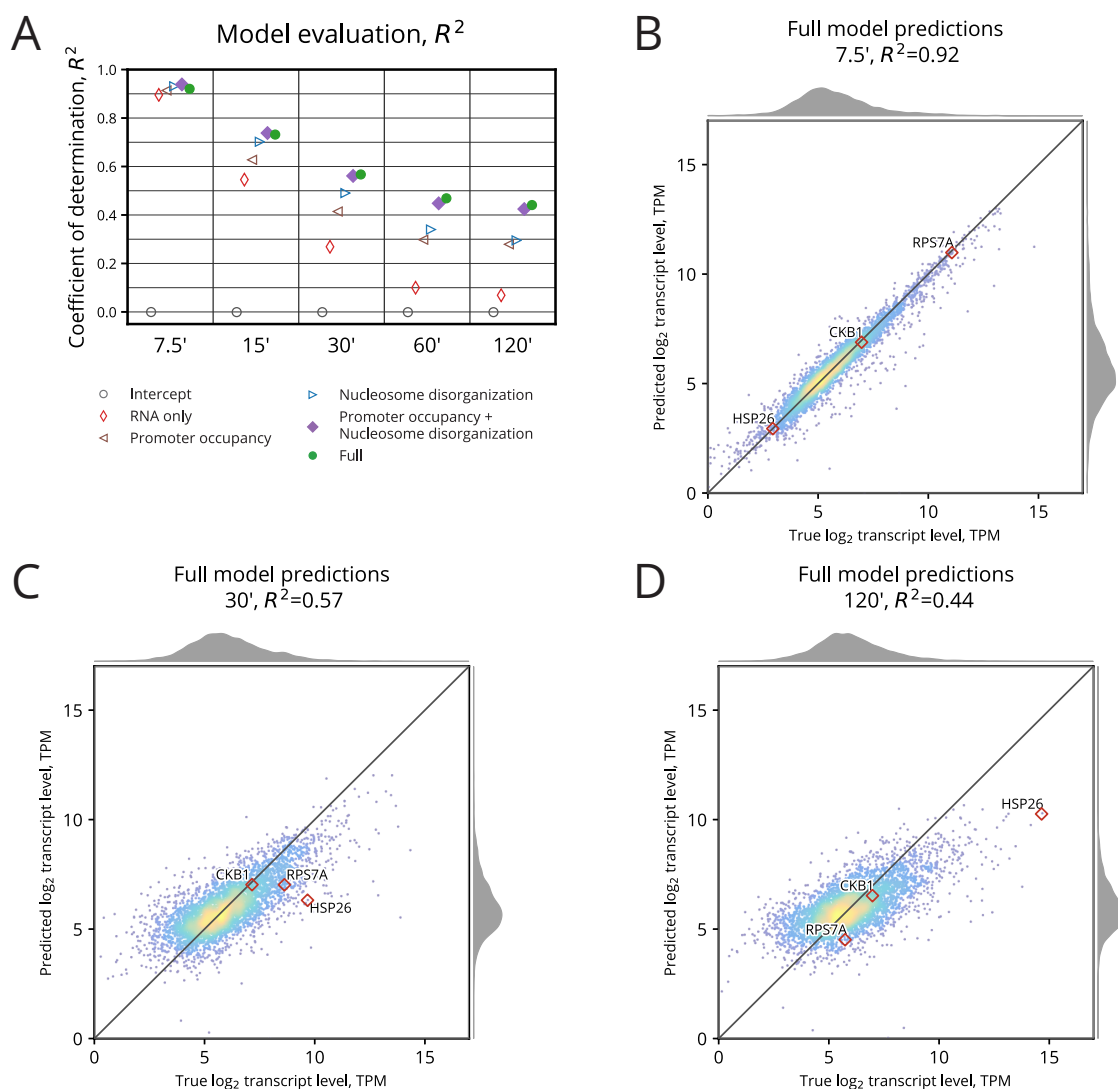


**Figure 8.** Chromatin occupancy dynamics are predictive of gene expression. **(A)** Comparison of each GP model’s performance using its coefficient of determination,  $R^2$ . The Full model incorporating all chromatin features and 0 min transcript level outperforms all other models for 30–120 min. Later time points rely less on 0 min transcript level for prediction, so the marginal gain in statistical power between features becomes more evident. **(B)** Comparison between true and predicted  $\log_2$  transcript level for the Full model after 7.5 min. Most genes are well predicted using 0 min transcript level. **(C)** Full model predictions at 30 min. Predictions remain well correlated, but less than at 7.5 min. **(D)** Full model predictions at 120 min. After two full hours have elapsed, transcript level predictions have become a bit less correlated, but still,  $R^2$  remains 0.44.

## 559 **References**

- 560 Ashburner M, Ball CA, Blake JA, Botstein D, Butler H, Cherry JM, Davis AP, Dolinski K,  
561 Dwight SS, Eppig JT, Harris MA, Hill DP, Issel-Tarver L, Kasarskis A, Lewis S, Matese  
562 JC, Richardson JE, Ringwald M, Rubin GM, Sherlock G. 2000. Gene Ontology: Tool  
563 for the unification of biology. *Nat. Genet.* **25**: 25–29.
- 564 Barbey R, Baudouin-Cornu P, Lee TA, Rouillon A, Zarzov P, Tyers M, Thomas D. 2005.  
565 Inducible dissociation of SCF(Met30) ubiquitin ligase mediates a rapid transcrip-  
566 tional response to cadmium. *EMBO J.* **24**: 521–532.
- 567 Belsky JA, MacAlpine HK, Lubelsky Y, Hartemink AJ, MacAlpine DM. 2015. Genome-  
568 wide chromatin footprinting reveals changes in replication origin architecture in-  
569 duced by pre-RC assembly. *Genes Dev.* **29**: 212–224.
- 570 Benesch JLP, Aquilina JA, Baldwin AJ, Rekas A, Stengel F, Lindner RA, Basha E, Devlin  
571 GL, Horwitz J, Vierling E, Carver JA, Robinson CV. 2010. The quaternary organi-  
572 zation and dynamics of the molecular chaperone HSP26 are thermally regulated.  
573 *Chem. Biol.* **17**: 1008–1017.
- 574 Benjamini Y, Hochberg Y. 1995. Controlling the false discovery rate: A practical and  
575 powerful approach to multiple testing. *J. R. Stat. Soc. Series B Stat. Methodol.* **57**:  
576 289–300.
- 577 Blaiseau PL, Thomas D. 1998. Multiple transcriptional activation complexes tether the  
578 yeast activator Met4 to DNA. *EMBO J.* **17**: 6327–6336.
- 579 Blaiseau PL, Isnard AD, Surdin-Kerjan Y, Thomas D. 1997. Met31p and Met32p, two  
580 related zinc finger proteins, are involved in transcriptional regulation of yeast sulfur  
581 amino acid metabolism. *Mol. Cell. Biol.* **17**: 3640–3648.

- 582 Boy-Marcotte E, Lagniel G, Perrot M, Bussereau F, Boudsocq A, Jacquet M, Labarre J.  
583 1999. The heat shock response in yeast: Differential regulations and contributions  
584 of the Msn2p/Msn4p and Hsf1p regulons. *Mol. Microbiol.* **33**: 274–283.
- 585 Brahma S, Henikoff S. 2019. RSC-associated subnucleosomes define MNase-sensitive  
586 promoters in yeast. *Mol. Cell* **73**: 238–249.e3.
- 587 Brennan RJ, Schiestl RH. 1996. Cadmium is an inducer of oxidative stress in yeast.  
588 *Mutat. Res.* **356**: 171–178.
- 589 Brogaard K, Xi L, Wang JP, Widom J. 2012. A map of nucleosome positions in yeast at  
590 base-pair resolution. *Nature* **486**: 496–501.
- 591 Camblong J, Iglesias N, Fickentscher C, Dieppois G, Stutz F. 2007. Antisense RNA sta-  
592 bilization induces transcriptional gene silencing via histone deacetylation in *S. cere-*  
593 *visiae*. *Cell* **131**: 706–717.
- 594 Carrillo E, Ben-Ari G, Wildenhain J, Tyers M, Grammentz D, Lee TA. 2012. Character-  
595 izing the roles of Met31 and Met32 in coordinating Met4-activated transcription in  
596 the absence of Met30. *Mol. Biol. Cell* **23**: 1928–1942.
- 597 Cashikar AG, Duennwald M, Lindquist SL. 2005. A chaperone pathway in protein dis-  
598 aggregation: Hsp26 alters the nature of protein aggregates to facilitate reactivation  
599 by Hsp104. *J. Biol. Chem.* **280**: 23869–23875.
- 600 Chen J, Pederson DS. 1993. A distal heat shock element promotes the rapid response to  
601 heat shock of the HSP26 gene in the yeast *Saccharomyces cerevisiae*. *J. Biol. Chem.*  
602 **268**: 7442–7448.
- 603 Chereji RV, Ocampo J, Clark DJ. 2017. MNase-sensitive complexes in yeast: Nucleo-  
604 somes and non-histone barriers. *Mol. Cell* **65**: 565–577.e3.

- 605 Cormier L, Barbey R, Kuras L. 2010. Transcriptional plasticity through differential  
606 assembly of a multiprotein activation complex. *Nucleic Acids Res.* **38**: 4998–5014.
- 607 Dormer UH, Westwater J, McLaren NF, Kent NA, Mellor J, Jamieson DJ. 2000.  
608 Cadmium-inducible expression of the yeast GSH1 gene requires a functional sulfur-  
609 amino acid regulatory network. *J. Biol. Chem.* **275**: 32611–32616.
- 610 Faller P, Kienzler K, Krieger-Liszkay A. 2005. Mechanism of Cd<sup>2+</sup> toxicity: Cd<sup>2+</sup>  
611 inhibits photoactivation of Photosystem II by competitive binding to the essential  
612 Ca<sup>2+</sup> site. *Biochim. Biophys. Acta* **1706**: 158–164.
- 613 Fauchon M, Lagniel G, Aude JC, Lombardia L, Soularue P, Petat C, Marguerie G, Sen-  
614 tenac A, Werner M, Labarre J. 2002. Sulfur sparing in the yeast proteome in response  
615 to sulfur demand. *Mol. Cell* **9**: 713–723.
- 616 Franzmann TM, Menhorn P, Walter S, Buchner J. 2008. Activation of the chaperone  
617 Hsp26 is controlled by the rearrangement of its thermosensor domain. *Mol. Cell* **29**:  
618 207–216.
- 619 Gardarin A, Chédin S, Lagniel G, Aude JC, Godat E, Catty P, Labarre J. 2010. Endo-  
620 plasmic reticulum is a major target of cadmium toxicity in yeast. *Mol. Microbiol.* **76**:  
621 1034–1048.
- 622 Geisberg JV, Moqtaderi Z, Fan X, Oszolak F, Struhl K. 2014. Global analysis of mRNA  
623 isoform half-lives reveals stabilizing and destabilizing elements in yeast. *Cell* **156**:  
624 812–824.
- 625 Grant CE, Bailey TL, Noble WS. 2011. FIMO: scanning for occurrences of a given motif.  
626 *Bioinformatics* **27**: 1017–1018.
- 627 Hartwig A. 2001. Zinc finger proteins as potential targets for toxic metal ions: Differ-  
628 ential effects on structure and function. *Antioxid. Redox Signal.* **3**: 625–634.

- 629 Henikoff JG, Belsky JA, Krassovsky K, MacAlpine DM, Henikoff S. 2011. Epigenome  
630 characterization at single base-pair resolution. *Proc. Natl. Acad. Sci. U. S. A.* **108**:  
631 18318–18323.
- 632 Hosiner D, Gerber S, Lichtenberg-Fraté H, Glaser W, Schüller C, Klipp E. 2014. Impact  
633 of acute metal stress in *Saccharomyces cerevisiae*. *PLoS One* **9**: e83330.
- 634 Huisinga KL, Pugh BF. 2004. A genome-wide housekeeping role for TFIID and a highly  
635 regulated stress-related role for SAGA in *Saccharomyces cerevisiae*. *Mol. Cell* **13**:  
636 573–585.
- 637 Jin YH, Clark AB, Slebos RJC, Al-Refai H, Taylor JA, Kunkel TA, Resnick MA, Gordenin  
638 DA. 2003. Cadmium is a mutagen that acts by inhibiting mismatch repair. *Nat. Genet.*  
639 **34**: 326–329.
- 640 Jin YH, Dunlap PE, McBride SJ, Al-Refai H, Bushel PR, Freedman JH. 2008. Global  
641 transcriptome and deletome profiles of yeast exposed to transition metals. *PLoS*  
642 *Genet.* **4**: e1000053.
- 643 Kaiser P, Flick K, Wittenberg C, Reed SI. 2000. Regulation of transcription by ubiqui-  
644 tination without proteolysis: Cdc34/SCF(Met30)-mediated inactivation of the tran-  
645 scription factor Met4. *Cell* **102**: 303–314.
- 646 Kawahata M, Masaki K, Fujii T, Iefuji H. 2006. Yeast genes involved in response to  
647 lactic acid and acetic acid: Acidic conditions caused by the organic acids in *Sac-*  
648 *charomyces cerevisiae* cultures induce expression of intracellular metal metabolism  
649 genes regulated by Aft1p. *FEMS Yeast Res.* **6**: 924–936.
- 650 Kim TS, Liu CL, Yassour M, Holik J, Friedman N, Buratowski S, Rando OJ. 2010. RNA  
651 polymerase mapping during stress responses reveals widespread nonproductive tran-  
652 scription in yeast. *Genome Biol.* **11**: R75.

- 653 Klopfenstein DV, Zhang L, Pedersen BS, Ramírez F, Warwick Vesztrocy A, Naldi A,  
654 Mungall CJ, Yunes JM, Botvinnik O, Weigel M, Dampier W, Dessimoz C, Flick P,  
655 Tang H. 2018. GOATOOLS: A Python library for Gene Ontology analyses. *Sci. Rep.*  
656 **8**: 10872.
- 657 Kornienko AE, Guenzl PM, Barlow DP, Pauler FM. 2013. Gene regulation by the act of  
658 long non-coding RNA transcription. *BMC Biol.* **11**: 59.
- 659 Krogan NJ, Cagney G, Yu H, Zhong G, Guo X, Ignatchenko A, Li J, Pu S, Datta N,  
660 Tikuisis AP, Punna T, Peregrín-Alvarez JM, Shales M, Zhang X, Davey M, Robinson  
661 MD, Paccanaro A, Bray JE, Sheung A, Beattie B, Richards DP, Canadien V, Lalev  
662 A, Mena F, Wong P, Starostine A, Canete MM, Vlasblom J, Wu S, Orsi C, Collins SR,  
663 Chandran S, Haw R, Rilstone JJ, Gandi K, Thompson NJ, Musso G, St Onge P, Ghanny  
664 S, Lam MHY, Butland G, Altaf-Ul AM, Kanaya S, Shilatifard A, O’Shea E, Weissman  
665 JS, Ingles CJ, Hughes TR, Parkinson J, Gerstein M, Wodak SJ, Emili A, Greenblatt JF.  
666 2006. Global landscape of protein complexes in the yeast *saccharomyces cerevisiae*.  
667 *Nature* **440**: 637–643.
- 668 Kubik S, Bruzzone MJ, Albert B, Shore D. 2017. A reply to “MNase-sensitive complexes  
669 in yeast: Nucleosomes and non-histone barriers,” by Chereji et al. *Mol. Cell* **65**:  
670 578–580.
- 671 Kulaeva OI, Hsieh FK, Studitsky VM. 2010. RNA polymerase complexes cooperate to  
672 relieve the nucleosomal barrier and evict histones. *Proc. Natl. Acad. Sci. U. S. A.* **107**:  
673 11325–11330.
- 674 Kuras L, Cherest H, Surdin-Kerjan Y, Thomas D. 1996. A heteromeric complex contain-  
675 ing the centromere binding factor 1 and two basic leucine zipper factors, Met4 and  
676 Met28, mediates the transcription activation of yeast sulfur metabolism. *EMBO J.*  
677 **15**: 2519–2529.

- 678 Kuras L, Rouillon A, Lee T, Barbey R, Tyers M, Thomas D. 2002. Dual regulation of  
679 the Met4 transcription factor by ubiquitin-dependent degradation and inhibition of  
680 promoter recruitment. *Mol. Cell* **10**: 69–80.
- 681 Langmead B, Trapnell C, Pop M, Salzberg SL. 2009. Ultrafast and memory-efficient  
682 alignment of short DNA sequences to the human genome. *Genome Biol.* **10**: R25.
- 683 Lee CK, Shibata Y, Rao B, Strahl BD, Lieb JD. 2004. Evidence for nucleosome depletion  
684 at active regulatory regions genome-wide. *Nat. Genet.* **36**: 900–905.
- 685 Lenstra TL, Benschop JJ, Kim T, Schulze JM, Brabers NACH, Margaritis T, van de Pasch  
686 LAL, van Heesch SAAC, Brok MO, Groot Koerkamp MJA, Ko CW, van Leenen D,  
687 Sameith K, van Hooff SR, Lijnzaad P, Kemmeren P, Hentrich T, Kobor MS, Bura-  
688 towski S, Holstege FCP. 2011. The specificity and topology of chromatin interaction  
689 pathways in yeast. *Mol. Cell* **42**: 536–549.
- 690 Lubliner S, Keren L, Segal E. 2013. Sequence features of yeast and human core pro-  
691 moters that are predictive of maximal promoter activity. *Nucleic Acids Res.* **41**: 5569–  
692 5581.
- 693 MacIsaac KD, Wang T, Gordon DB, Gifford DK, Stormo GD, Fraenkel E. 2006. An im-  
694 proved map of conserved regulatory sites for *Saccharomyces cerevisiae*. *BMC Bioin-*  
695 *formatics* **7**: 113.
- 696 McIsaac RS, Petti AA, Bussemaker HJ, Botstein D. 2012. Perturbation-based analysis  
697 and modeling of combinatorial regulation in the yeast sulfur assimilation pathway.  
698 *Mol. Biol. Cell* **23**: 2993–3007.
- 699 Miller C, Schwalb B, Maier K, Schulz D, Dümcke S, Zacher B, Mayer A, Sydow J, Mar-  
700 cinowski L, Dölken L, Martin DE, Tresch A, Cramer P. 2011. Dynamic transcriptome  
701 analysis measures rates of mRNA synthesis and decay in yeast. *Mol. Syst. Biol.* **7**:  
702 458.

- 703 Miller KA, DiDone L, Krysan DJ. 2010. Extracellular secretion of overexpressed  
704 glycosylphosphatidylinositol-linked cell wall protein Utr2/Crh2p as a novel protein  
705 quality control mechanism in *saccharomyces cerevisiae*. *Eukaryot. Cell* **9**: 1669–  
706 1679.
- 707 Momose Y, Iwahashi H. 2001. Bioassay of cadmium using a DNA microarray: Genome-  
708 wide expression patterns of *Saccharomyces cerevisiae* response to cadmium. *Environ.*  
709 *Toxicol. Chem.* **20**: 2353–2360.
- 710 Nadal-Ribelles M, Solé C, Xu Z, Steinmetz LM, de Nadal E, Posas F. 2014. Control of  
711 Cdc28 CDK1 by a stress-induced lncRNA. *Mol. Cell* **53**: 549–561.
- 712 Nocetti N, Whitehouse I. 2016. Nucleosome repositioning underlies dynamic gene  
713 expression. *Genes Dev.* **30**: 660–672.
- 714 Ouni I, Flick K, Kaiser P. 2010. A transcriptional activator is part of an SCF ubiquitin  
715 ligase to control degradation of its cofactors. *Mol. Cell* **40**: 954–964.
- 716 Park D, Morris AR, Battenhouse A, Iyer VR. 2014. Simultaneous mapping of tran-  
717 script ends at single-nucleotide resolution and identification of widespread promoter-  
718 associated non-coding RNA governed by TATA elements. *Nucleic Acids Res.* **42**: 3736–  
719 3749.
- 720 Patton EE, Peyraud C, Rouillon A, Surdin-Kerjan Y, Tyers M, Thomas D. 2000.  
721 SCF(Met30)-mediated control of the transcriptional activator Met4 is required for  
722 the G(1)-S transition. *EMBO J.* **19**: 1613–1624.
- 723 Pedregosa F, Varoquaux G, Gramfort A, Michel V, Thirion B, Grisel O, Blondel M, Pret-  
724 tenhofer P, Weiss R, Dubourg V, Vanderplas J, Passos A, Cournapeau D, Brucher M,  
725 Perrot M, Duchesnay E. 2011. Scikit-learn: Machine learning in Python. *Journal of*  
726 *Machine Learning Research* **12**: 2825–2830.

- 727 Pereira Y, Lagniel G, Godat E, Baudouin-Cornu P, Junot C, Labarre J. 2008. Chromate  
728 causes sulfur starvation in yeast. *Toxicol. Sci.* **106**: 400–412.
- 729 Petti AA, McIsaac RS, Ho-Shing O, Bussemaker HJ, Botstein D. 2012. Combinatorial  
730 control of diverse metabolic and physiological functions by transcriptional regulators  
731 of the yeast sulfur assimilation pathway. *Mol. Biol. Cell* **23**: 3008–3024.
- 732 Presnyak V, Alhusaini N, Chen YH, Martin S, Morris N, Kline N, Olson S, Weinberg D,  
733 Baker KE, Graveley BR, Collier J. 2015. Codon optimality is a major determinant of  
734 mRNA stability. *Cell* **160**: 1111–1124.
- 735 Rabani M, Levin JZ, Fan L, Adiconis X, Raychowdhury R, Garber M, Gnirke A, Nusbaum  
736 C, Hacohen N, Friedman N, Amit I, Regev A. 2011. Metabolic labeling of RNA un-  
737 covers principles of RNA production and degradation dynamics in mammalian cells.  
738 *Nat. Biotechnol.* **29**: 436–442.
- 739 Ramachandran S, Ahmad K, Henikoff S. 2017. Transcription and remodeling produce  
740 asymmetrically unwrapped nucleosomal intermediates. *Mol. Cell* **68**: 1038–1053.e4.
- 741 Reja R, Vinayachandran V, Ghosh S, Pugh BF. 2015. Molecular mechanisms of riboso-  
742 mal protein gene coregulation. *Genes Dev.* **29**: 1942–1954.
- 743 Rhee HS, Pugh BF. 2012. Genome-wide structure and organization of eukaryotic pre-  
744 initiation complexes. *Nature* **483**: 295–301.
- 745 Schwabish MA, Struhl K. 2004. Evidence for eviction and rapid deposition of histones  
746 upon transcriptional elongation by RNA polymerase II. *Mol. Cell. Biol.* **24**: 10111–  
747 10117.
- 748 Sharma SK, Goloubinoff P, Christen P. 2008. Heavy metal ions are potent inhibitors of  
749 protein folding. *Biochem. Biophys. Res. Commun.* **372**: 341–345.

- 750 Shivaswamy S, Iyer VR. 2008. Stress-dependent dynamics of global chromatin remod-  
751 eling in yeast: Dual role for SWI/SNF in the heat shock stress response. *Mol. Cell.*  
752 *Biol.* **28**: 2221–2234.
- 753 Smale ST, Kadonaga JT. 2003. The RNA polymerase II core promoter. *Annu. Rev.*  
754 *Biochem.* **72**: 449–479.
- 755 Susek RE, Lindquist S. 1990. Transcriptional derepression of the *Saccharomyces cere-*  
756 *visiae* HSP26 gene during heat shock. *Mol. Cell. Biol.* **10**: 6362–6373.
- 757 Swamy KBS, Lin CH, Yen MR, Wang CY, Wang D. 2014. Examining the condition-  
758 specific antisense transcription in *S. cerevisiae* and *S. paradoxus*. *BMC Genomics* **15**:  
759 521.
- 760 Teves SS, Henikoff S. 2011. Heat shock reduces stalled RNA polymerase II and nucle-  
761 osome turnover genome-wide. *Genes Dev.* **25**: 2387–2397.
- 762 The Gene Ontology Consortium. 2019. The Gene Ontology Resource: 20 years and still  
763 GOing strong. *Nucleic Acids Res.* **47**: D330–D338.
- 764 Till P, Mach RL, Mach-Aigner AR. 2018. A current view on long noncoding RNAs in  
765 yeast and filamentous fungi. *Appl. Microbiol. Biotechnol.* **102**: 7319–7331.
- 766 Toesca I, Nery CR, Fernandez CF, Sayani S, Chanfreau GF. 2011. Cryptic transcrip-  
767 tion mediates repression of subtelomeric metal homeostasis genes. *PLoS Genet.* **7**:  
768 e1002163.
- 769 Treger JM, Schmitt AP, Simon JR, McEntee K. 1998. Transcriptional factor mutations  
770 reveal regulatory complexities of heat shock and newly identified stress genes in  
771 *Saccharomyces cerevisiae*. *J. Biol. Chem.* **273**: 26875–26879.
- 772 Tripuraneni V, Memisoglu G, Zhu W, Tran T, Hartemink AJ, Haber JE, MacAlpine DM.  
773 2019. Local nucleosome dynamics and eviction following a double-strand break are

774 reversible by NHEJ-mediated repair in the absence of DNA replication. *bioRxiv* page  
775 866673.

776 Vance KW, Ponting CP. 2014. Transcriptional regulatory functions of nuclear long non-  
777 coding RNAs. *Trends Genet.* **30**: 348–355.

778 Venters BJ, Wachi S, Mavrich TN, Andersen BE, Jena P, Sinnamon AJ, Jain P, Rolleri NS,  
779 Jiang C, Hemeryck-Walsh C, Pugh BF. 2011. A comprehensive genomic binding map  
780 of gene and chromatin regulatory proteins in *Saccharomyces*. *Mol. Cell* **41**: 480–492.

781 Vinayachandran V, Reja R, Rossi MJ, Park B, Rieber L, Mittal C, Mahony S, Pugh BF.  
782 2018. Widespread and precise reprogramming of yeast protein-genome interactions  
783 in response to heat shock. *Genome Res.* **28**: 357–366.

784 Virtanen P, Gommers R, Oliphant TE, Haberland M, Reddy T, Cournapeau D, Burovski  
785 E, Peterson P, Weckesser W, Bright J, van der Walt SJ, Brett M, Wilson J, Jarrod  
786 Millman K, Mayorov N, Nelson ARJ, Jones E, Kern R, Larson E, Carey C, Polat İ,  
787 Feng Y, Moore EW, Vand erPlas J, Laxalde D, Perktold J, Cimrman R, Henriksen I,  
788 Quintero EA, Harris CR, Archibald AM, Ribeiro AH, Pedregosa F, van Mulbregt P,  
789 Contributors S. 2020. SciPy 1.0: Fundamental algorithms for scientific computing in  
790 Python. *Nature Methods* **17**: 261–272.

791 Wagner GP, Kin K, Lynch VJ. 2012. Measurement of mRNA abundance using RNA-seq  
792 data: RPKM measure is inconsistent among samples. *Theory Biosci.* **131**: 281–285.

793 Ward JH. 1963. Hierarchical grouping to optimize an objective function. *J. Am. Stat.*  
794 *Assoc.* **58**: 236–244.

795 Weiner A, Chen HV, Liu CL, Rahat A, Klien A, Soares L, Gudipati M, Pfeffner J, Regev  
796 A, Buratowski S, Pleiss JA, Friedman N, Rando OJ. 2012. Systematic dissection of  
797 roles for chromatin regulators in a yeast stress response. *PLoS Biol.* **10**: e1001369.

- 798 Weiner A, Hsieh THS, Appleboim A, Chen HV, Rahat A, Amit I, Rando OJ, Friedman N.  
799 2015. High-resolution chromatin dynamics during a yeast stress response. *Mol. Cell*  
800 **58**: 371–386.
- 801 Wiederhold E, Gandhi T, Permentier HP, Breitling R, Poolman B, Slotboom DJ. 2009.  
802 The yeast vacuolar membrane proteome. *Mol. Cell. Proteomics* **8**: 380–392.
- 803 Wilhelm BT, Marguerat S, Watt S, Schubert F, Wood V, Goodhead I, Penkett CJ, Rogers  
804 J, Bähler J. 2008. Dynamic repertoire of a eukaryotic transcriptome surveyed at  
805 single-nucleotide resolution. *Nature* **453**: 1239–1243.
- 806 Yang E, van Nimwegen E, Zavolan M, Rajewsky N, Schroeder M, Magnasco M, Darnell  
807 Jr JE. 2003. Decay rates of human mRNAs: Correlation with functional characteris-  
808 tics and sequence attributes. *Genome Res.* **13**: 1863–1872.